J. Cent. South Univ. (2022) 29: 1761−1777
DOI: https://doi.org/10.1007/s11771-022-5047-0

Springer

A 3D graphene/polyimide fiber framework with improved thermal conductivity and mechanical performance

WANG Xian-peng(王先鹏)[1], HU Ai-ping(胡爱平)[1]*, CHEN Xiao-hua(陈小华)[1]*, LIU Ji-lei(刘继磊)[1], LI Yan-hua(李艳花)[2], LI Chuan-yi(李传议)[1], WANG Han(王涵)[1], TANG Qun-li(唐群力)[1]

1. College of Materials Science and Engineering, Hunan University, Changsha 410082, China;
2. College of Materials and Chemistry Engineering, Hunan Institute of Technology, Hengyang 421002, China

Abstract: The integration of electronic components and the popularity of flexible devices have come up with higher expectations for the heat dissipation capability and comprehensive mechanical performance of thermal management materials. In this work, after the modification of polyimide (PI) fibers through oxidation and amination, the obtained PDA@OPI fibers (polydopamine (PDA)-modified pre-oxidized PI fibers) with abundant amino groups were mixed into graphene oxide (GO) to form uniform GO-PDA@OPI composites. Followed by evaporation, carbonization, graphitization and mechanical compaction, the G-gPDA@OPI films with a stable three-dimensional (3D) long-range interconnected covalent structure were built. In particular, due to the rich covalent bonds between GO layers and PDI@OPI fibers, the enhanced synergistic graphitization promotes an ordered graphitized structure with less interlayer distance between adjacent graphene sheets in composite film. As a result, the optimized G-gPDA@OPI film displays an improved tensile strength of 78.5 MPa, tensile strain of 19.4% and thermal conductivity of 1028 W/(m·K). Simultaneously, it also shows superior flexibility and high resilience. This work provides an easily-controlled and relatively low-cost route for fabricating multifunctional graphene heat dissipation films.

Key words: graphene film; modified polyimide fiber; polydopamine; thermal conductivity; mechanical properties

Cite this article as: WANG Xian-peng, HU Ai-ping, CHEN Xiao-hua, LIU Ji-lei, LI Yan-hua, LI Chuan-yi, WANG Han, TANG Qun-li. A 3D graphene/polyimide fiber framework with improved thermal conductivity and mechanical performance [J]. Journal of Central South University, 2022, 29(6): 1761−1777. DOI: https://doi.org/10.1007/s11771-022-5047-0.

1 Introduction

With the advancement of electronic equipment and communication technology, thermal management materials with excellent heat dissipation capacity are required to remove the heat in time during the operation of electronic components [1−5]. Notably, the popularity of wearable flexible devices has put forward higher requirements for the mechanical properties of heat dissipation materials [6−8]. For instance, their high tensile strength and superior folding resistance can ensure their processability and compatibility with flexible substrates [9−12]. In addition, the heat dissipation materials with remarkable resilience are

Foundation item: Projects(51971089, 51872087) supported by the National Natural Science Foundation of China; Project(2020JJ5021) supported by the Natural Science Foundation of Hunan Province, China; Project(kq1804010) supported by the Major Science and Technology Program of Changsha, China
Received date: 2022-02-26; **Accepted date:** 2022-04-22
Corresponding author: HU Ai-ping, PhD, Professor; E-mail: hudaaipinghu@126.com; ORCID: https://orcid.org/0000-0003-3572-3850; CHEN Xiao-hua, PhD, Professor; E-mail: xiaohuachen@hnu.edu.cn; ORCID: https://orcid.org/0000-0003-1054-1487

able to tightly adhere to the thermal interface materials when subjected to a certain packaging pressure, so that the interface thermal resistance can be effectively reduced [13−16]. Therefore, to meet the needs of the next-generation smart devices, it is urgent to find a type of material with both excellent heat dissipation and comprehensive mechanical properties.

Graphene, a two-dimensional (2D) carbon nano-material composed of sp^2-hybridized carbon atoms, is considered as the most ideal material for heat dissipation owing to its outstanding thermal conductivity and mechanical properties [17−18]. As the graphene-based macroscopic components, graphene films (GFs) are usually obtained by carbonization or graphitization of graphene oxide films (GOFs), which can be fabricated through simple vacuum filtration, wetting coating, or evaporation of self-assembled graphene oxide (GO) suspension [19−20]. Through high-temperature treatment, oxygen-containing functional groups of GO sheets can be removed and their defects can be repaired, which would boost the transport of phonons [21−23]. However, after annealing, due to the weak linkage between graphene platelets, the GFs generally show the limited thermal conductivity and tensile properties [24−26].

To strengthen the interaction between graphene platelets, some strategies such as in-situ polymerization or recombination with one-dimensional (1D) nanomaterials have been adopted in recent studies [27−29]. For instance, WANG et al [30] introduced polyacrylonitrile to weld adjacent GO sheets, with thermal conductivity of 1629 W/(m·K) and tensile strength of 46 MPa. ZOU et al [31] prepared a covalently crosslinked graphene/carbon nanotube composite film with thermal conductivity of 1597 W/(m·K) and tensile strength of 67.5 MPa. Although the thermal performance has been obviously improved through the bridging between graphene sheets, the tensile strength is still limited because of the intrinsic brittleness of the carbonized reinforcement and the weak connection between the 1D short-range materials.

The flexibility and resilience of thermal management materials take important roles in the application of the packaging conditions. Whereas, the weak interaction between graphene layers is disadvantageous for the uniform stress distribution during bending the GFs, which will lead to poor flexibility [32 − 33]. Moreover, the GFs typically show low resilience ratio due to the enhanced van der Waals forces between graphene sheets after mechanically pressing [34]. Up to date, some studies pointed out that these problems could be tackled through the construction of three-dimensional (3D) hybrid network to some extent [35−37]. For instance, KONG et al [38] prepared an ultra-flexible graphite-carbon fiber composite paper, which could be bent 6000 times without fracture. FENG et al [39] obtained a 3D hierarchy with a rebound rate of 78% by growing carbon nanotubes among layers of graphite sheets, which was attributed to the fact that the adhesion effect originating from van der Waals force can be inhibited owing to the support of 1D carbon nanotubes in the normal direction. However, GFs with both fine flexibility and high resilience were rarely reported so far. Hence, it is still a great challenge to fabricate a multifunctional heat dissipation film with excellent comprehensive performance due to their various enhancement mechanisms of these properties (thermal conductivity, tensile strength, flexibility and resilience).

Aromatic polyimide (PI) fibers were usually used to weave a reinforcing network inside the GFs owing to the following advantages. On the one hand, the long PI fibers with high modulus and superior flexibility tend to be entangled with each other so as to build a strong framework. On the other hand, the considerable carbon residue rate and high-quality graphite products will be achieved after graphitization on account of the ordered structure of PI molecules [40].

Based on the analysis above, in this work, at first, PI fibers were modified by oxidation and amination to obtain PDA@OPI fibers with excellent dispersibility and surface activity. Afterwards, they were complexed with GO sheets to construct a 3D interconnected graphene composite film (G-gPDA@OPI) after graphitization. The superiorities of this ingenious structural design are illustrated as follows: 1) The graphitized PDA@OPI fibers stitch adjacent graphene sheets through

covalent bond to facilitate load transfer and energy dissipation, which is beneficial for heightening the thermal conductivity and tensile strength of the composite films. 2) The 3D long-range interconnected structure can ensure smooth absorption and release of energy, similar to elastic mattress made of metal mesh and fabric, which results in outstanding flexibility and resilience. 3) The synergistic effect between GO sheets and PI fibers during the graphitization is conductive to fully repair defects and form more intact crystal structure. Importantly, this synergistic effect is further strengthened by enhanced interfacial coupling via covalent interaction. As a result, the G-gPDA@OPI film is expected to show a high thermal conductivity and excellent mechanical properties.

2 Experimental

2.1 Preparation of samples

Potassium permanganate ($KMnO_4$), concentrated sulfuric acid (H_2SO_4, 98%) and hydrogen peroxide (H_2O_2, 30%) were obtained from Sinopharm Chemical Reagent Co. Ltd., China. Dopamine (DA, 98%) and tris(hydroxymethyl) aminomethane were acquired from Shanghai Aladdin Biochemical Technology Co., Ltd., China. Natural graphite flake (325 mesh) was obtained from Sigma-Aldrich Trading Co., Ltd. PI fiber (average length of 3 mm) was purchased from SHINO New Materials Tech Co., Ltd., China.

1) Synthesis of GO. GO suspension was synthesized by modified Hummer's method as we reported previously [41−43].

2) Preparation of PDA@OPI fibers. PI fibers were calcined at 450 °C for 3 h in an air atmosphere to enhance their surface activity to obtain OPI fibers. 2 g of OPI fibers was dispersed in tris-HCl buffer solution (500 mL, pH=8.5) with ultrasonication for 5 min. 1 g of DA was added into the OPI fiber dispersion solution and then the mixture was vigorously stirred for 24 h at ambient temperature to polymerize DA. The solution was filtrated to remove the solvent, and the product PDA@OPI fibers, were washed with deionized water several times and dried at 80 °C.

3) Fabrication of G-gPDA@OPI films. At first, the GO suspension (4 mg/mL) and the PDA@OPI fibers with different mass fractions were evenly mixed and reacted by agitation at 60 °C for 4 h to acquire the GO-PDA@OPI dispersion. After the GO-PDA@OPI films were synthesized by evaporation of solvent in a Petri dish at 45 °C for several days, they were carbonized at 1000 °C for 2 h and graphitized at 3000 °C for 1 h in an Ar atmosphere. Finally, through mechanical compacting at 30 MPa for 2 h, the G-gPDA@OPI films were fabricated. As comparison, the G-gPI films and the G-gOPI films were prepared with the same procedure.

2.2 Materials characterization

Fourier transform infrared spectroscopy (FTIR) was conducted on Nicolet 6700 with a range of 400−4000 cm^{-1} at room temperature. The chemical environment and composition of the composite films were analyzed adopting X-ray photoelectron spectroscopy (XPS, ESCALAB 250 Xi). The X-ray diffraction (XRD) results of the samples were obtained employing a Bruker D8 advance X-ray diffractometer (Cu-K_α, λ =0.154 nm). The Raman spectra were measured on a WITec alpha 300 Raman microscope with a 532 nm laser source to assess the degree of crystallinity and defect information of the samples. The field-emission scanning electron microscope (FESEM, S4800) was used to observe the surface and cross-section morphology of the composite films.

2.3 Performance test

The mechanical properties were recorded on a Shimadzu AGS-X tester at room temperature and ambient humidity. The gauge length and load speed were 5 mm and 1 mm/min, respectively. The strips employed for tensile test were 2 mm wide and 30 mm long. The electrical conductivity of samples was measured using the four-point probe (Four-probe tester, SX-1934). Bending tests were operated by previous method [44]. The diameter of the mandrel was 1.0 mm. The thermal diffusivity was tested by the laser flash method on a LFA 447 apparatus (NETZSCH, Germany) at room temperature. The thermal conductivity (K) was calculated by Eq. (1):

$$K = \rho \cdot c_p \cdot \alpha \quad (1)$$

where ρ denotes the density of the sample; c_p (1.15 J/(g·K), Figure S1) represents the specific heat capacity tested via a NETZSCH 214 Polyma differential scanning calorimeter at 25 °C; and α symbolizes the thermal diffusivity. The density (ρ) was measured according to $\rho = mV^{-1}$, where m and V symbolize the mass and volume of the sample in serval, respectively. The thickness was obtained through averaging the thicknesses at 5 different locations from the SEM images of the sample.

3 Results and discussion

3.1 Preparation mechanism

Figure 1 illustrates the fabrication procedure of the G-gPDA@OPI composite films.

1) The modification of PI fibers. As seen in Figure S2, PI fibers exhibit poor dispersibility in water due to their entanglement and chemical inertness, which is unfavorable for them to uniformly complex with GO sheets, as well as tightly combine among PI and GO. Therefore, at first, the PI fibers were oxidized in an air atmosphere at 450 ℃. As shown in Figure S3, the surface of OPI fibers is coarser than that of PI fibers, which can be originated from the modification of oxygen-containing functional groups (Table S1 and Figure S4). Afterwards, to further enhance the affinity between GO sheets and OPI fibers, PDA was chosen to modify OPI fibers since dopamine can form stable non-covalent interaction with most inorganic and organic substances through self-polymerization [45–46]. From Figure S3(c), it can be seen that OPI fibers are evidently covered with PDA layers. Moreover, the augment in nitrogen atom content and C—N peak area (Table S1 and Figure S4) further demonstrates the successful deposition of PDA on OPI fibers. From Figures S2(b) and (c), it can be known that both OPI fibers and PDA@OPI fibers show prominent hydrophilicity.

2) The formation of uniform mixed film with PDA@OPI fibers and GO sheets. The PDA@OPI fibers with functional groups containing abundant N and O can be evenly mixed into GO solutions and they can undergo nucleophilic substitution reaction to form covalent bonds between them. Afterwards, through evaporation at 45 °C, the uniform GO-PDA@OPI film can be obtained.

3) The graphitization of GO-PDA@OPI film. GO-PDA@OPI films were carbonized at 1000 °C for 2 h and then graphitized at 3000 °C for 1 h in an Ar atmosphere. The tight coupling between PDA and OPI fibers will promote the rearrangement of interfacial carbon atoms in the process of graphitization, thereby forming continuous and

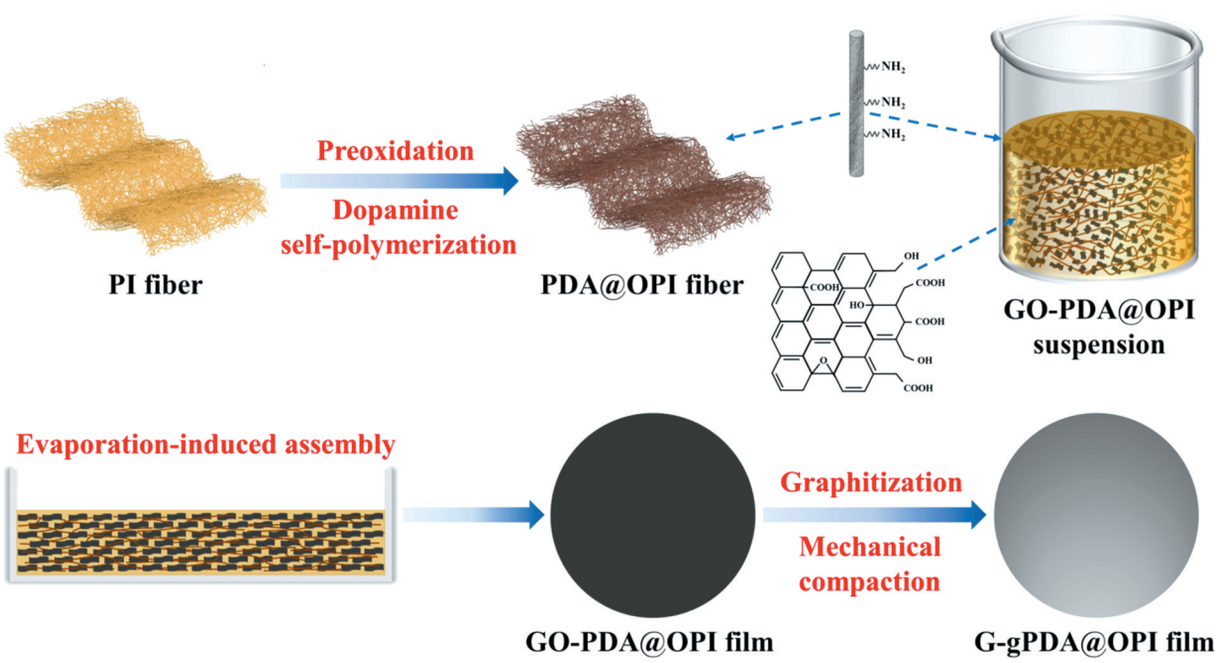

Figure 1 Fabrication process of G-gPDA@OPI films

complete covalent crystals [31]. At the same time, the high-quality graphite composite structures can be obtained due to the repair of defects.

4) The compaction of G-gPDA@OPI film. Through mechanical compacting at 30 MPa for 2 h, the G-gPDA@OPI composite films were fabricated.

3.2 Structure characteristics

FTIR spectroscopy was executed to reveal the interaction between components in composite films. As displayed in Figure 2(a), for GO film, the characteristic absorption peaks at 1723, 1619, 1224 and 1049 cm^{-1} correspond to the stretching vibrations of C═O, C═C, C—O and C—O—C groups, respectively. By contrast, for GO-PI-30% film, its intensity and width of the C═C peak are increased, which should be ascribed to the π-π interaction between GO and PI [47]. In addition, compared with GO film, for GO-PDA@OPI film, the intensities of the C—O—C and C—O groups are weakened, and the C═O peak is red shifted, which can be inferred as the chemical interaction between GO platelets and PDA@OPI fibers [48–50]. The results of XPS spectra can further verify the reaction between GO and PDA@OPI. As displayed in Figures 2(b) and (c), the N 1s spectra of PDA@OPI fiber can be divided into two peaks at 399.6 eV and 401.8 eV, which are assigned to C—N—C group of the PI fiber and —NH— group of the PDA, respectively. However, for GO-PDA@OPI-30% film, the obvious decrease of —NH— group area ratio and the appearance

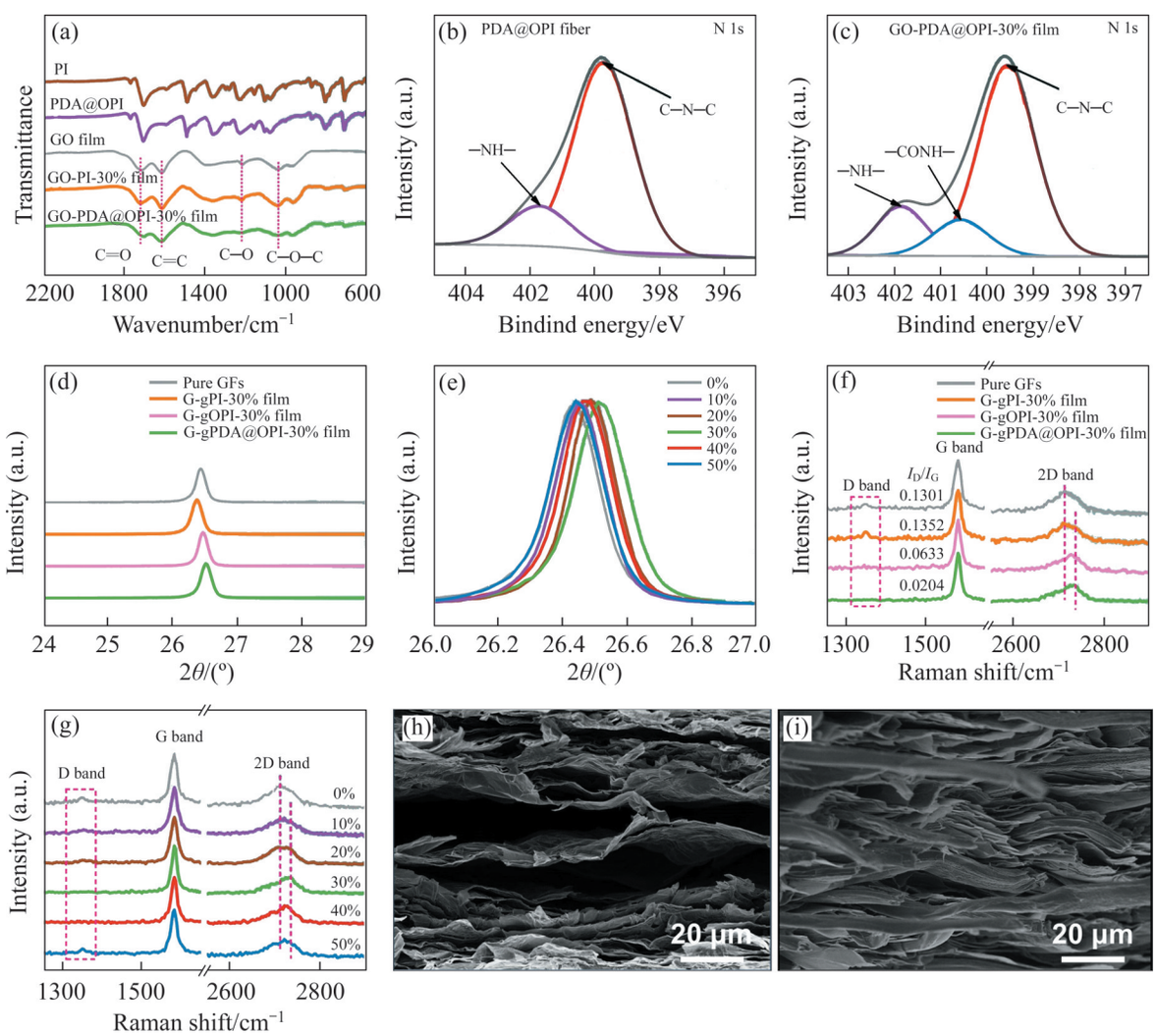

Figure 2 (a) FTIR spectra of samples; XPS N 1s spectra of (b) PDA@OPI fiber and (c) GO-PDA@OPI-30% film; (d) XRD patterns and (f) Raman spectra of G-gPDA@OPI films with different compositions; (e) XRD patterns and (g) Raman spectra of films with different PDA@OPI fiber contents; Cross-sectional SEM images of (h) pure GFs and (i) G-gPDA@OPI-30% film

of —CONH— peak (401.8 eV) can be found. Combined with the results of FTIR spectroscopy, it indicates the formation of stable amide bonds by the reaction between the oxygen-containing functional group of GO and the amino group of PDA@OPI fibers.

The XRD pattern can be conducted to analyze the structural transformation of the composite films. From Figure 2(d) and Table S2, it can be seen that the 2θ peaks corresponding to (002) plane of graphite for G-gPI-30% film, pure GFs, G-gOPI-30% film and G-gPDA@OPI-30% film increase, successively. The G-gPI-30% film exhibits the highest crystal plane *d*-spacing among samples, which should result from its looser structure due to poor blending of unmodified PI fibers with GO sheets (Figures S5(a) and (d)). However, with the modification of PI fibers, the interaction between GO sheets and PI fibers is enhanced, so that the *d*-spacing of the composite films decreased. The lowest crystal plane *d*-spacing for the G-gPDA@OPI-30% film can be ascribed to the strong covalent interaction between gPDA@OPI fibers and graphene sheets. Notably, as shown in the Table S2, based on the Mering and Maire's equation [51], the calculated graphitization degrees of pure GFs, G-gOPI-30% film and G-gPDA@OPI-30% film are 81.4%, 89.2% and 95.3%, respectively. It can be explained by the synergistic effect between GO sheets and OPI fibers during the graphitization. In detail, on the one hand, because the OPI fibers are closely adhered to the GO sheets in the composite film (Figures S5(b) and (e)), the ordered planar structure of GO sheets can serve as a template to induce the nucleation of carbonized PI molecules during heat treatment [52]. On the other hand, the small molecules produced through the decomposition of PI can act as additional carbon and nitrogen sources to fill the vacancies in the graphene lattice and repair the flaws of graphene [53−54]. With the enhancement of the interfacial coupling between GO sheets and modified PI fibers, the synergistic graphitization will be strengthened, leading to a more integral crystal structure. In addition, the XRD patterns of the G-gPDA@OPI composite films with different content of PDA@OPI fiber are shown in Figure 2(e) and Table S3. The peak position of samples increases with the content of PDA@OPI fiber heightening from 0 to 30%, which can originate from the uniform intercalation of gPDA@OPI fibers in graphene sheets. It further indicates that the gPDA@OPI fibers play a significant role in the graphitization of composites. However, the excessive gPDA@OPI fibers tend to aggregate between graphene sheets when the mass fraction of the PDA@OPI fibers continues to raise, leading to an expansion of the lattice space.

Raman spectra are used to evaluate the flaws information of the graphene composite films. As presented in Figure 2(f), for pure GFs, an evident D band can be found, which indicates that the defects remain existed after annealing. For the G-gPI-30% film, the augment of I_D/I_G value illustrates the increase of edge defects, originating from agglomerated PI fibers. By contrast, for the G-gOPI-30% film and the G-gPDA@OPI-30% film, the D bands can hardly be detectable. It indicates that a more perfect crystal structure can be formed due to the homogeneous dispersion and the tight interactions through covalent bonds between GO sheets and modified PI fibers, which should be attributed to the fact that modified PI fibers accelerate the graphitization process. In particular, compared with G-gOPI-30% film, the G-gPDA@OPI-30% film shows a lower I_D/I_G value. It further proves that the improvement of the interfacial coupling between GO sheets and OPI fibers through covalent interaction can enhance the synergistic graphitization effect. In addition, in comparison to the pure GFs, the 2D band of the G-gPDA@OPI-30% film shifts from 2712 to 2734 cm^{-1}, which illustrates a higher interlayer cohesive energy of order AB Bernal stacking graphene [55]. It suggests that the covalent interaction between layers is advantageous to enhance the combination among stacked graphene sheets. Additionally, the effect of PDA@OPI fiber content on the Raman spectra of the composite films is shown in Figure 2(g). As the content of PDA@OPI fibers is added up to 30%, D band almost disappears, manifesting that the incorporation of PDA@OPI fibers is in favor of acquiring a more complete graphitic structure. Simultaneously, the 2D peak is blue shifted, owing to the covalent connection between graphene sheets

and gPDA@OPI fibers. On the contrary, with the mass fraction of the fibers surge from 30% to 50%, the D peak reappears and the 2D peak position gradually returns, which should be contributed to the extra defects produced from aggregated gPDA@OPI fibers. The results of Raman spectra are in accordance with those of the XRD patterns.

SEM is employed to describe the microstructure of the composite films. From the cross-sectional view of pure GFs (Figure 2(h)), it can be seen that large gaps exist between graphene sheets. By contrast, for the G-gPDA@OPI-30% film (Figure 2(i)), a dense and well-ordered hierarchical structure can be noticed. The micrographic difference of two composite films can be explained as follow: during heating treatment of the precursors of composite films, the decomposition of oxygen-containing functional groups of GO will generate gases. In the GO-PDA@OPI film, abundant micropores are formed at the cross-linked interface of PDA@OPI fibers and GO sheets, through which the gases can escape quickly (Figure S6(a)). At the same time, the rich defects in the polymers can also act as gas-escaping channels, suppressing the expansion effect of GO sheets during annealing process [56]. However, in pure GO film, a dense layer structure can be found due to the superior self-assembly ability of GO sheets (Figure S6(b)). Therefore, it is difficult for a large amount of gas to escape, resulting in a loose structure after graphitization.

3.3 Thermal conductivity

The influence of different modified PI fibers on thermal conductivity of graphene composite films is displayed in Figure 3(a) and Table S4. The thermal conductivity of pure GFs is only 868 W/(m·K), originating from the weak connection between graphene sheets. The poorer conductivities of G-gPI-30% film than pure GFs suggests that the aggregated gPI fibers introduce more defects to restrain the transfer of phonons. In contrast, both of

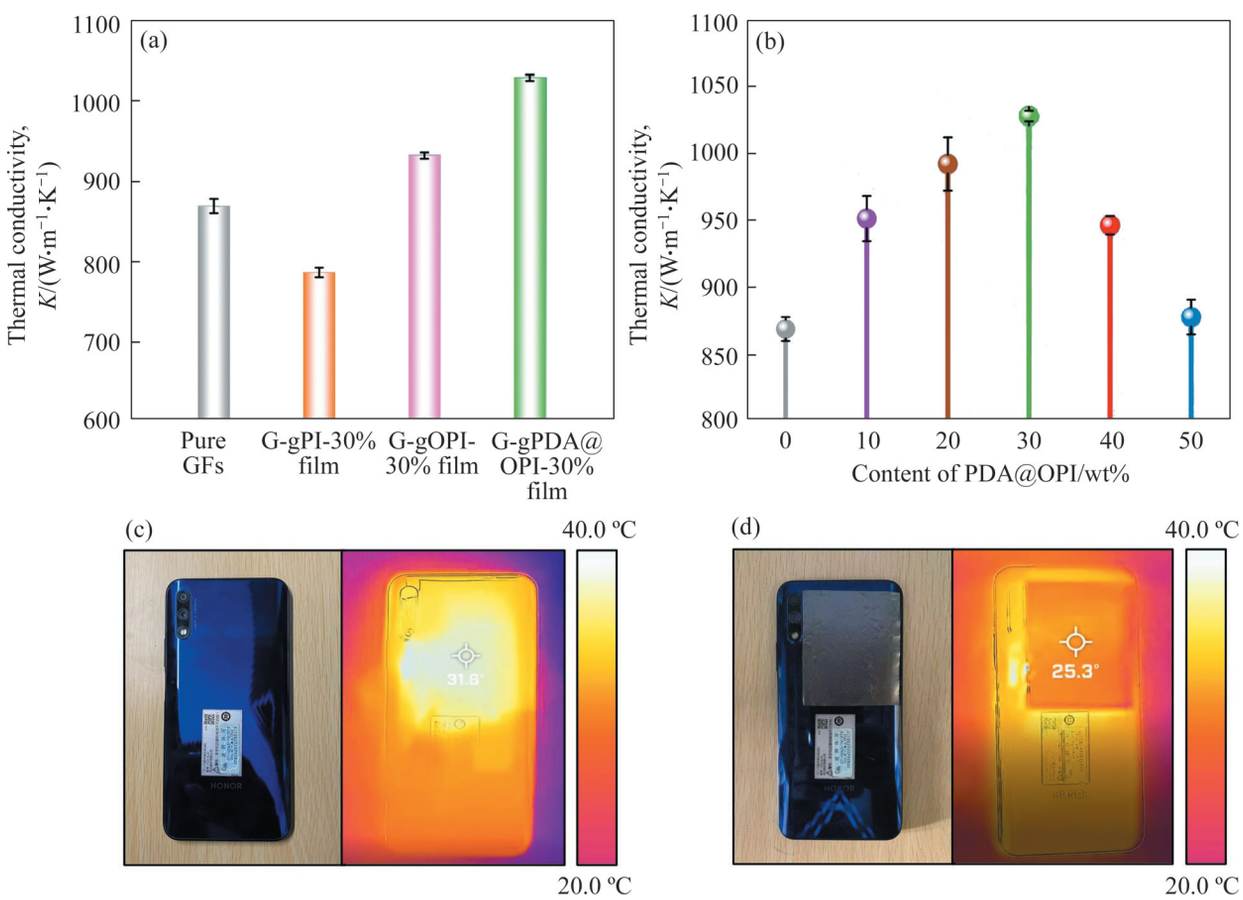

Figure 3 (a) Thermal conductivity of films with different compositions; (b) Thermal conductivity of G-gPDA@OPI films with different PDA@OPI fiber contents; (c, d) Heat dissipation application of G-gPDA@OPI-30% film in a smart phone

the G-gOPI-30% film and the G-gPDA@OPI-30% film show more satisfying thermal conductivity, which is owing to the bridging adjacent between graphene sheets by graphitized modified fiber. As expected, since the gPDA@OPI fibers and graphene sheets are connected by the indurative covalent interaction, it comports the best thermal conductivity (1028 W/(m·K). From Figure 3(b) and Table S5, the effect of different content of PDA@OPI fiber can be seen. The thermal conductivity of the composite films is improved gradually with the addition of PDA@OPI fiber from 0 to 30%, while they show a drop tendency with further growth of PDA@OPI fiber content. It further proves that covalent linkage between graphene sheets and gPDA@OPI fibers plays a key role to form a stable 3D interconnected structure with excellent crystallinity and facilitates the transport of phonons effectively. The aggregation of excess gPDA@OPI fibers in the composite films constitutes a number of pores inside the composite films, which will reduce crystal integrity and disrupt the orderly arrangement of graphene platelets so as to decrease the conductivity. Therefore, the composite film with 30% PDA@OPI fibers displays the best thermal conductivity, which is consistent with the results of XRD and Raman spectra. In order to test the actual cooling efficiency of the samples, the G-gPDA@OPI-30% film was used for the heat dissipation of the smartphone when running high-power software, as illustrated in Figures 3(c) and (d). Due to the excellent heat transfer performance of G-gPDA@OPI-30% film, the heat generated by the operation of the mobile phone can be emitted timely. As a result, the surface temperature of the mobile phone case was maintained at about 25.3 °C, which is of great significance to ensure the efficient operation and service life of the electronic equipment.

3.4 Mechanical properties

The tensile properties of the composite films were measured on a universal electronic testing machine. The variation law of the tensile properties of the composite films is slightly distinguished from that of the thermal conductivity due to the different reinforcement mechanism. As displayed in Figures 4(a) and (b) and Table S6, for pure GFs, the tensile strength, the maximum strain rate and toughness are only 30.2 MPa, 2.1% and 0.74 MJ/m^3 respectively, due to the loose structure. For the G-gPI-30% film, because the entangled network of gPI fibers inhibits the detachment of graphene platelets and the curled gPI fibers can preferentially straighten when the composites are subjected to tension, manifesting higher strength of extension and ultimate stretch length than pure GFs. Regrettably, due to the poor dispersion of the gPI fibers in the G-gPI-30% film and the weak interaction between gPI fibers and graphene sheets, the enhancement of the tensile performance is limited. By contrast, the G-gOPI-30% film and the G-gPDA@OPI-30% film exhibit much better tensile strength, which is attributed to the uniform dissipation of stress promoted by the feasible blending effect between gOPI fibers and graphene sheets. In particular, for the G-gPDA@OPI-30% film, interlayer covalent structures can be constructed so that it shows the best tensile properties. Based on this, the content of PDA@OPI fibers in composite films plays an important part in the tensile performance of the G-gPDA@OPI films (Figures 4(c)−(e) and Table S7). As the amount of PDA@OPI fiber increases from 0 to 30%, the composite films show a better tensile performance and can withstand more strain, which is attributed to the strong 3D covalent network. However, the tensile performance becomes poorer due to the destruction of the structural integrity by excess gPDA@OPI fibers. Inspiringly, the optimized G-gPDA@OPI-30% film shows a tensile strength up to 78.5 MPa and a toughness of 8.73 MJ/m^3 when it is at 19.4% of the ultimate strain. Based on the analysis above, the formation of covalent cross-linking structure is available for the dissipation of energy so as to improve the tensile performance.

The indentation test was applied to explore the mechanical response of the G-gPDA@OPI-30% film, as depicted in Figure 4(f). Under a load of 0.3 mN, the penetration depth remained at 490 nm. The results make clear that the elastic modulus of the specimen is 0.38 GPa and the rebound rate is as high as 39.2%. Its low compressive modulus originates from the limited original density (1.49 g/cm^3). The high rebound rate (1.6 times that of pure GFs (Figure S7)) of the G-gPDA@OPI-30%

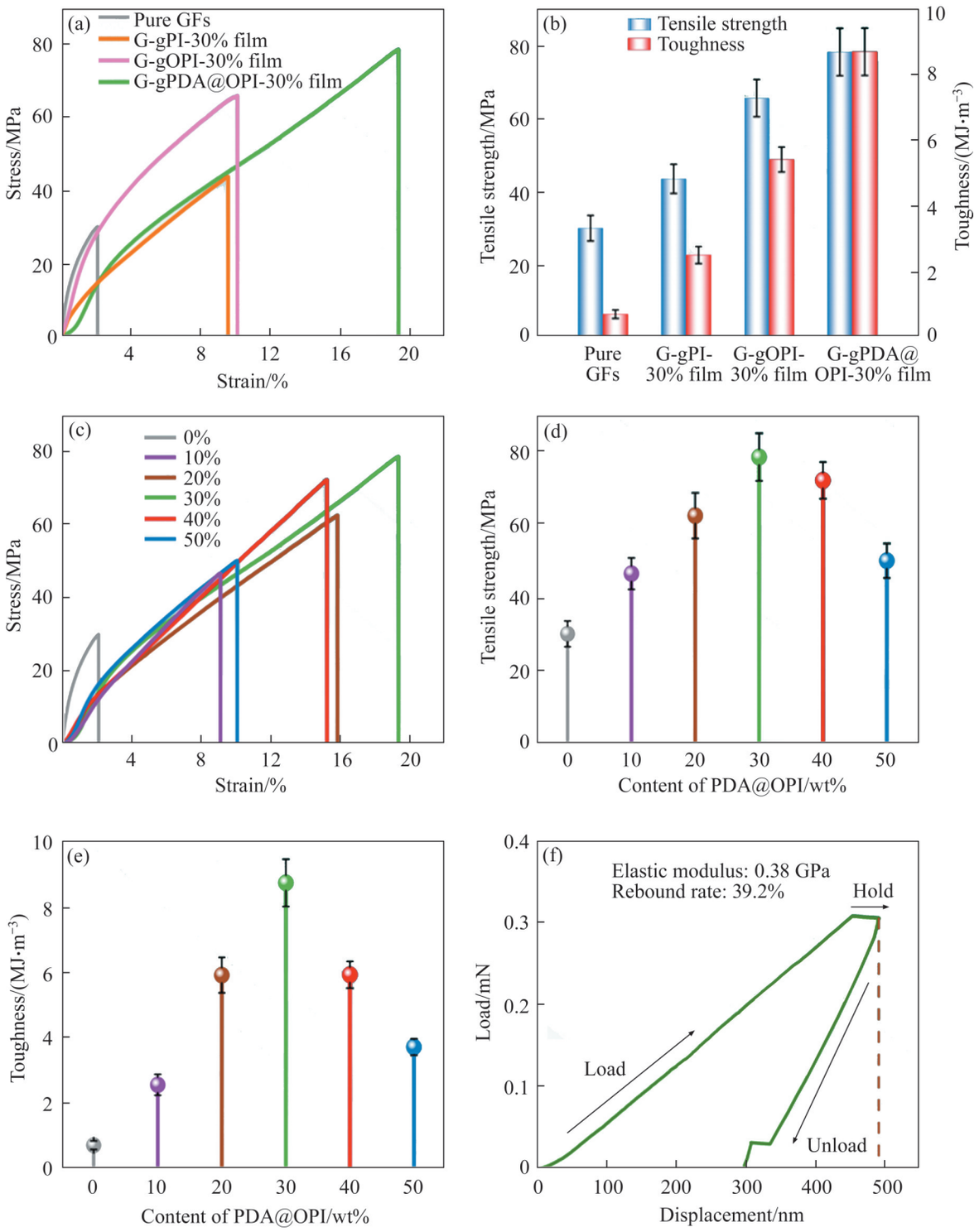

Figure 4 (a) Stress−strain curves and (b) tensile strength and toughness of films with different compositions; (c) Stress−strain curves, (d) tensile strength and (e) toughness of G-gPDA@OPI films with different PDA@OPI fiber contents; (f) Load−displacement curve for G-gPDA@OPI-30% film

film depends on distinctive 3D covalent cross-linked structure. The gPDA@OPI fibers are entangled with each other and tightly covered by graphene platelets, which can make sure the macroscopic overall deformation instead of dissociating between the various components when compressed. As a result, the stored elastic energy is easily released after unloading, promoting the composite film to return to its original state.

To evaluate the bending ability and folding

endurance of the composite films, we firstly recorded the variations of the surface morphology of the G-gPDA@OPI-30% film during folding-release cycles, which is displayed in Figures 5(a)–(e). The film displays a silver-gray metallic luster owing to the complete repair of microscopic defects. Notably, it reveals superior bending resistance. When it was folded in half, its surface could be restored through smoothing. Furthermore, a more accurate mold mentioned in our previous work [44], was adopted to further assess its flexibility. As shown in Figure 5(f), when it is folded 180° under a small bending radius of 1 mm, it remains almost unchanged excellent electrical conductivity after 4000 bending cycles, confirming its outstanding ductility.

To further investigate the excellent folding resistance of the G-gPDA@OPI-30% film, based on the structural change during folding, we put forward a conceivable microscopic transformation theory (Figure 6). From its SEM image (Figure 2(i)), it can

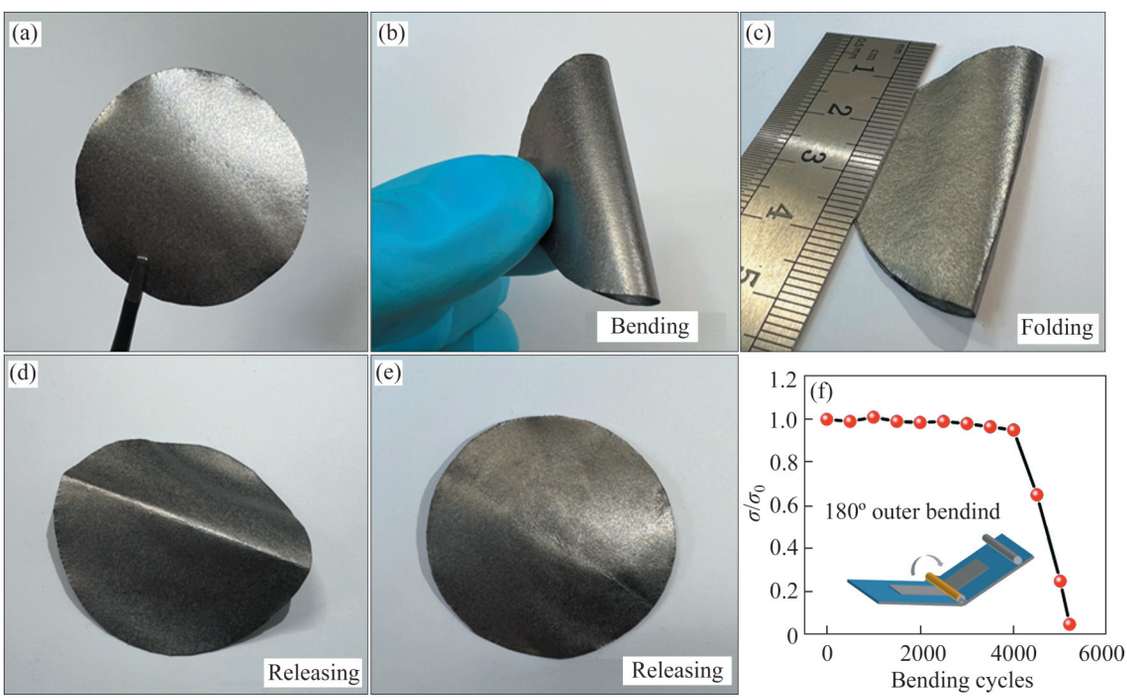

Figure 5 Optical pictures of G-gPDA@OPI-30% film in (a) pristine, (b) bending, (c) folding, (d) releasing and (e) recovering state; (f) Variation of electrical conductivity of G-gPDA@OPI-30% film under cyclic bending 5200 times

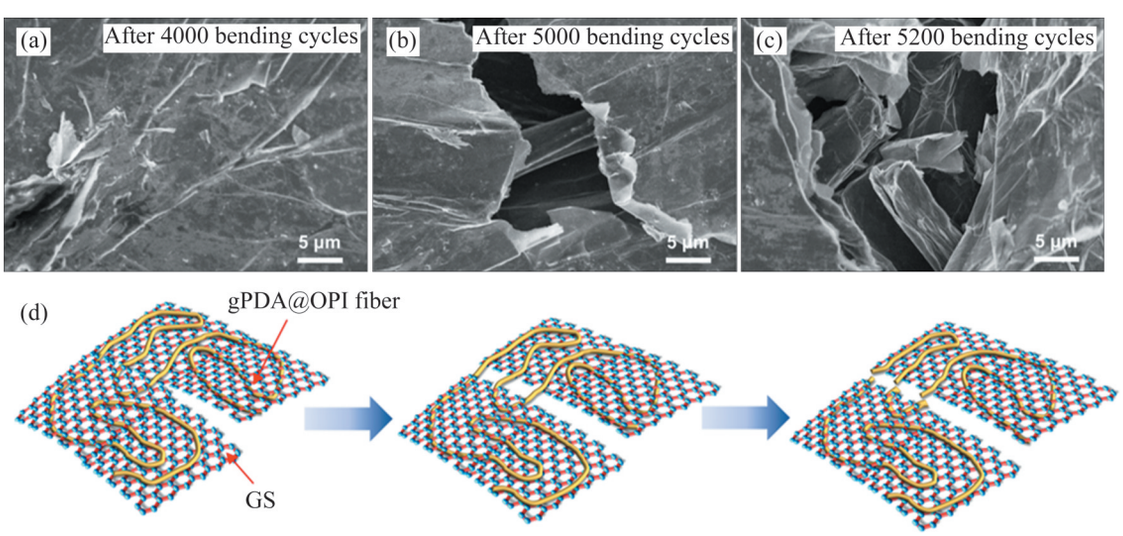

Figure 6 SEM images of the crack region when G-gPDA@OPI-30% film was bent (a) 4000 times, (b) 5000 times and (c) 5200 times; (d) Proposed explanation for the deformation process of G-gPDA@OPI-30% film

be found that the gPDA@OPI fibers are wound each other and evenly filled among graphene nanorings to form a strong 3D covalent cross-linked structure. During bending, the 3D long-range interconnected gPDA@OPI fibers network can absorb and release the stress uniformly so that the intact structure of the composite film can be sustained. In the cracked area, only a few wrinkles appear (Figure 6(a)), which is caused by the destruction of the van der Waals forces between the graphene sheets. Therefore, the electrical conductivity is not markedly weakened when the G-gPDA@OPI-30% film is bent 4000 times. With the increase of bending cycles, the covalent bonds between gPDA@OPI fibers and graphene platelets are broken and the graphene platelets separate from the fibers gradually (Figure 6(b)), leading to deterioration of electrical conductivity. Moreover, the magnified image of the fracture zone (Figure 6(c)) exhibits the fracture of gPDA@OPI fibers after 5200 bending times, predicting the failure of all properties of the composite film. It further indicates the significance of covalent bonds between GO and PI fibers to the thermal conductivity and the mechanical performce of the G-gPDA@OPI composite film.

4 Conclusions

In summary, through the oxidation and amination of PI fibers, the PDA@OPI fibers with abundant amino groups not only can be uniformly blended with GO in composite films, but also form rich covalent bonds between two components to weld the adjacent graphene sheets. As a result, the G-gPDA@OPI films with a strong 3D long-range uniformly interconnected structure were built. In the films, PI fibers provide microchannels for gas escape during the graphitization to enhance the horizontal orientation. Homogeneously, the covalent interaction further promotes the synergistic graphitization between PI and GO sheets and increases the crystallinity. Therefore, the transfer of load and dissipation of energy are facilitated effectively. As expected, the optimized G-gPDA@OPI-30% film exhibits excellent thermal and comprehensive mechanical properties. This work provides an effective way to design graphene heat dissipation films and also highly accelerate the application process of the G-gPDA@OPI films in the field of thermal management, especially for flexible electronic devices.

Appendix

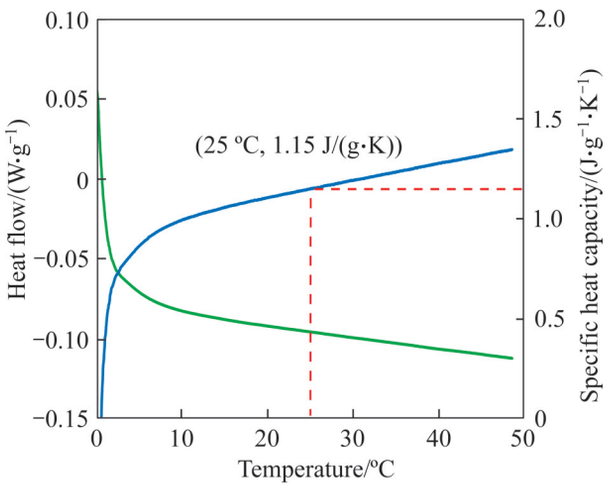

Figure S1 DSC curve of G-gPDA@OPI film

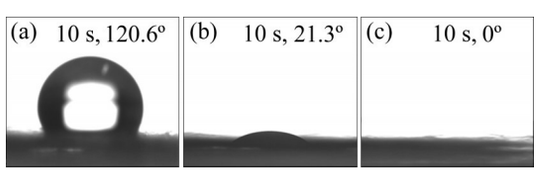

Figure S2 Wettability test of samples in water. Contact angles in wettability test of (a) PI fiber, (b) OPI fiber and (c) PDA@OPI fiber

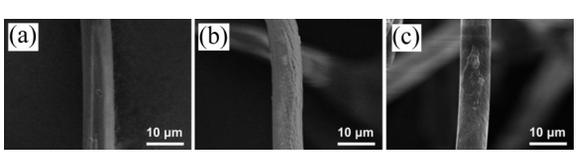

Figure S3 SEM images of (a) PI fiber, (b) OPI fiber and (c) PDA@OPI fiber

Table S1 Element molar fraction of PI, OPI and PDA@OPI fibers based on XPS analysis

Fiber type	*x*(C)/%	*x*(O)/%	*x*(N)/%
PI fiber	74.60	18.41	6.99
OPI fiber	72.09	21.47	6.43
PDA@OPI fiber	69.80	21.69	8.51

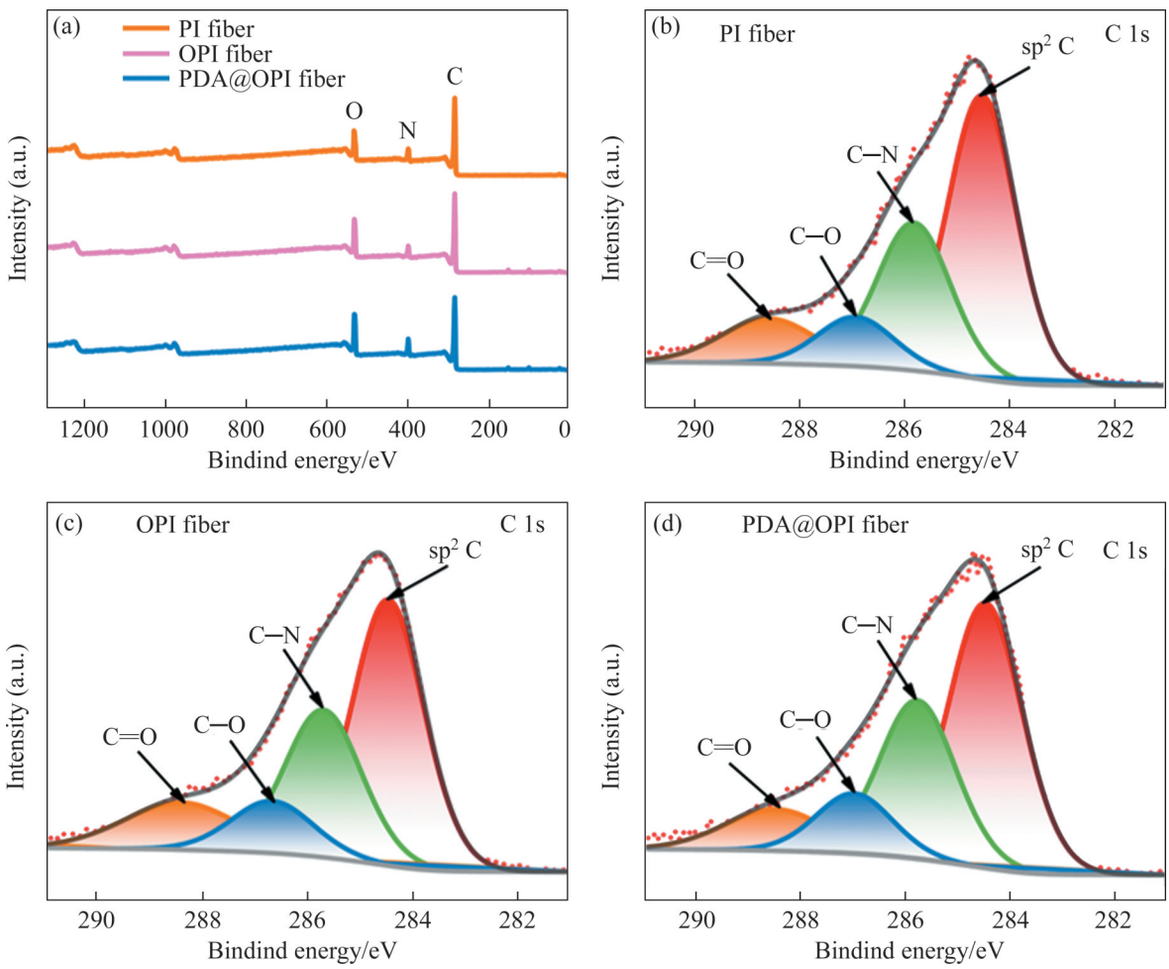

Figure S4 (a) XPS spectra of PI fiber, OPI fiber and PDA@OPI fiber; XPS C 1s spectra of (b) PI fiber, (c) OPI fiber and (d) PDA@OPI fiber

Table S2 Diffraction angle, *d*-spacing and graphitization degree of composite films with different compositions based on XRD curves

Sample	2θ/(°)	*d*-spacing/Å	Degree of graphitization/%
Pure GFs	26.429	3.3683	81.4%
G-gPI-30% film	26.374	3.3752	75.3%
G-gOPI-30% film	26.469	3.3633	89.2%
G-gPDA@OPI-30% film	26.512	3.3580	95.3%

Table S3 Diffraction angle and *d*-spacing of G-gPDA@OPI films with different PDA@OPI fiber content based on XRD curves

Mass fraction PDA@OPI/%	2θ/(°)	*d*-spacing/Å
0	26.429	3.3683
10	26.448	3.3660
20	26.487	3.3610
30	26.512	3.3580
40	26.470	3.3632
50	26.435	3.3676

Contributors

WANG Xian-peng: Concept, methodology, writing original draft. LIU Ji-lei, LI Yan-hua, LI Chuan-yi, WANG Han and TANG Qun-li: Investigation, validation. HU Ai-ping and CHEN Xiao-hua: Supervision, conceptualization, writing-reviewing and editing, funding acquisition.

Conflict of interest

The authors declare that they have no known competing financial interests or personal relationships that could have appeared to influence the work reported in this paper.

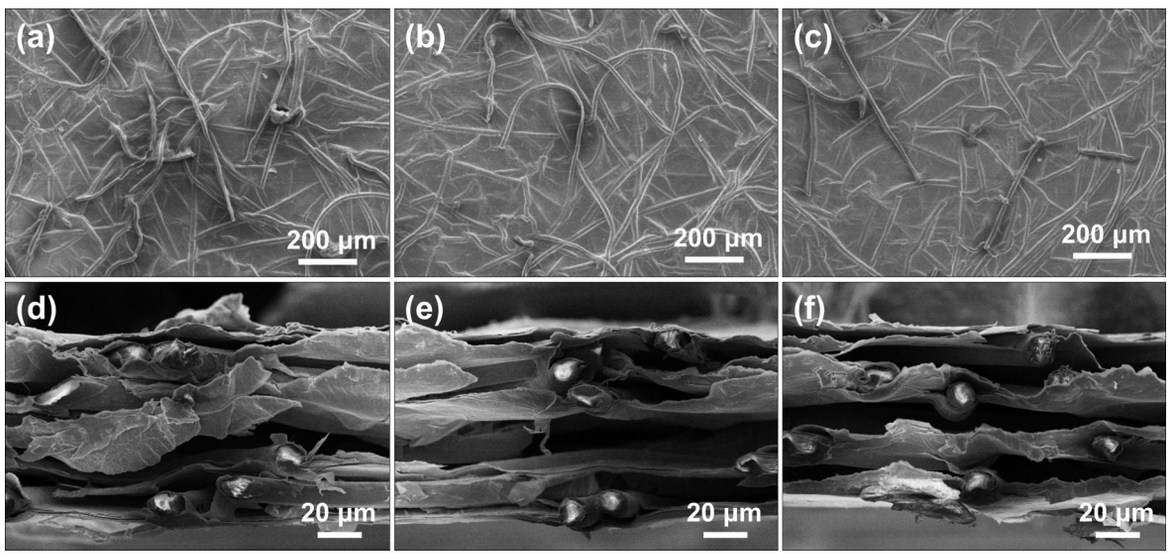

Figure S5 Surface SEM images of (a) GO-PI-30% film, (b) GO-OPI-30% film and (c) GO-PDA@OPI-30% film; Cross-sectional SEM images of (d) GO-PI-30% film, (e) GO-OPI-30% film and (f) GO-PDA@OPI-30% film

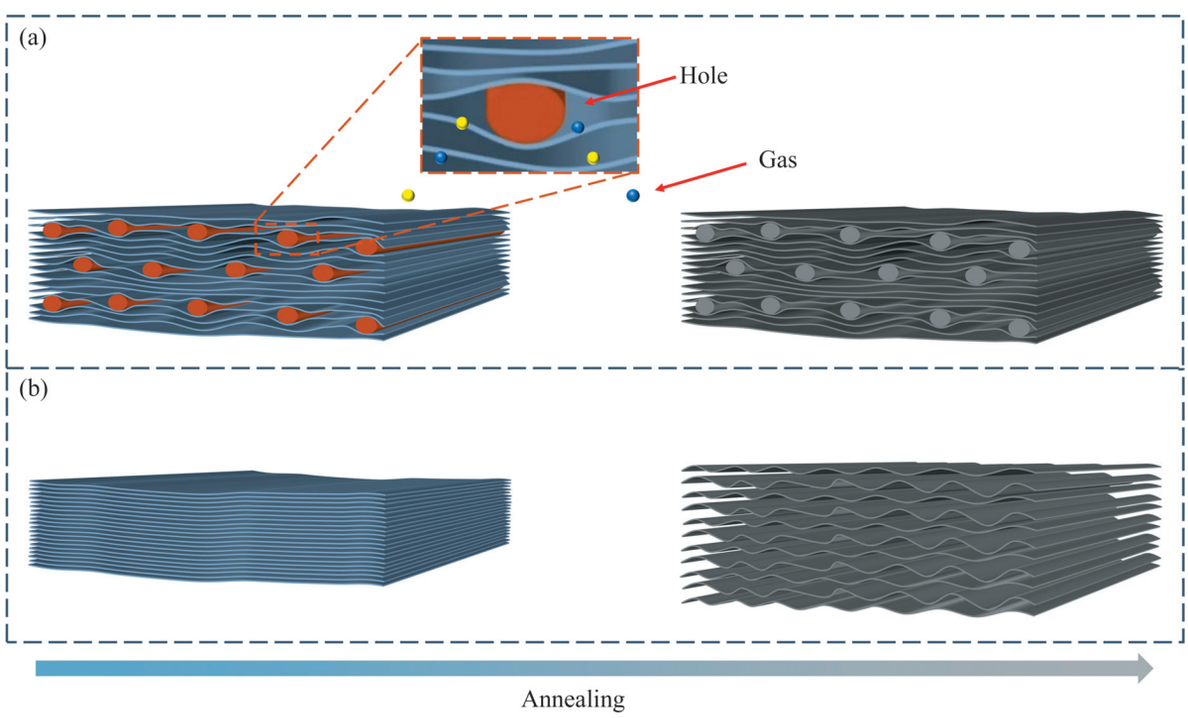

Figure S6 Structural transition of (a) GO-PDA@OPI film and (b) GO film during graphitization

Table S4 Density and thermal conductivity of pure GFs, G-gPI-30% film, G-gOPI-30% film and G-gPDA@OPI-30% film

Sample	Density, ρ/(g·cm^{-3})	Thermal diffusivity/(mm^2·s^{-1})	Thermal conductivity/(W·m^{-1}·K^{-1})
Pure GFs	1.48	510±5	868±9
G-gPI-30% film	1.48	461±3	785±6
G-gOPI-30% film	1.48	547±2	931±4
G-gPDA@OPI-30% film	1.49	600±2	1028±4

Table S5 Density and thermal conductivity of G-gPDA@OPI films with different PDA@OPI fiber contents

Mass fraction of PDA@OPI/%	Density, ρ/(g·cm^{-3})	Thermal diffusivity/(mm^2·s^{-1})	Thermal conductivity/(W·m^{-1}·K^{-1})
0	1.48	510±5	868±9
10	1.50	551±10	951±17
20	1.47	587±12	992±20
30	1.49	600±2	1028±4
40	1.49	552±4	946±7
50	1.50	509±8	877±13

Table S6 Thickness, tensile strength, ultimate tensile strain and toughness of pure GFs, G-gPI-30% film, G-gOPI-30% film and G-gPDA@OPI-30% film

Sample	Thickness/μm	Tensile strength/MPa	Ultimate tensile strain/%	Toughness/(MJ·m^{-3})
Pure GFs	45	30.2±3.5	2.1±0.5	0.74±0.13
G-gPI-30% film	60	43.8±4.0	9.6±1.2	2.54±0.26
G-gOPI-30% film	60	65.9±5.1	10.1±1.4	5.44±0.38
G-gPDA@OPI-30% film	55	78.5±6.5	19.4±2.8	8.73±0.72

Table S7 Thickness, tensile strength, ultimate tensile strain and toughness of G-gPDA@OPI films with different PDA@OPI fiber content

Mass fraction of PDA@OPI/%	Thickness/μm	Tensile strength/MPa	Ultimate tensile strain/%	Toughness/(MJ·m^{-3})
0	45	30.2±3.5	2.1±0.5	0.74±0.13
10	47	46.7±4.3	9.1±1.2	2.58±0.32
20	67	62.5±6.2	15.9±1.7	5.92±0.54
30	55	78.5±6.5	19.4±2.8	8.73±0.72
40	50	72.1±5.5	15.2±2.3	5.93±0.41
50	63	50.1±4.7	10.1±1.4	3.73±0.25

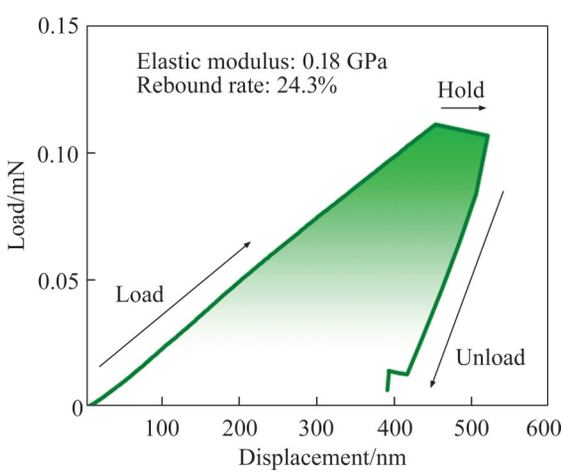

Figure S7 Load−displacement curve for pure GFs

References

[1] ZHANG Xiao-dong, GUO Yan, LIU Ying-jun, et al. Ultrathick and highly thermally conductive graphene films by self-fusion [J]. Carbon, 2020, 167: 249 − 255. DOI: 10.1016/j.carbon.2020.05.051.

[2] SONG Na, CAO Dong-lei, LUO Xian, et al. Highly thermally conductive polypropylene/graphene composites for thermal management [J]. Composites Part A: Applied Science and Manufacturing, 2020, 135: 105912. DOI: 10.1016/j.compositesa.2020.105912.

[3] PAN Zuo, WU Yan-hong, YUAN Hong, et al. Ascorbic acid-assisted defect healing and stack ordering of graphene films towards high power thermal dispersion [J]. Carbon, 2021, 182: 799−805. DOI: 10.1016/j.carbon.2021.06.058.

[4] LU Yun-hua, HAO Ji-can, XIAO Guo-yong, et al. Preparation and properties of in situ amino-functionalized graphene oxide/polyimide composite films [J]. Applied Surface Science, 2017, 422: 710−719. DOI: 10.1016/j.apsusc.2017.06.087.

[5] LIU Zi-xuan, WANG Xiao-long, HU Ai-ping, et al. 3D Se-doped NiCoP nanoarrays on carbon cloth for efficient alkaline hydrogen evolution [J]. Journal of Central South University, 2021, 28(8): 2345 − 2359. DOI: 10.1007/s11771-021-4774-y.

[6] LI Hao-liang, XIAO Shu-ning, YU Hong-liu, et al. A review of graphene-based films for heat dissipation [J]. New Carbon Materials, 2021, 36(5): 897−908. DOI: 10.1016/S1872-5805(21)60092-6.

[7] CHEN Shu-jing, WANG Qian-long, ZHANG Mao-mao,

et al. Scalable production of thick graphene film for next generation thermal management application [J]. Carbon, 2020, 167: 270−277. DOI: 10.1016/j.carbon.2020.06.030.

[8] LUO Fu-bin, WU Kun, SHI Jun, et al. Green reduction of graphene oxide by polydopamine to a construct flexible film: Superior flame retardancy and high thermal conductivity [J]. Journal of Materials Chemistry A, 2017, 5(35): 18542 − 18550. DOI: 10.1039/c7ta04740a.

[9] ZHUANG Ya-fang, ZHENG Kun, CAO Xin-yu, et al. Flexible graphene nanocomposites with simultaneous highly anisotropic thermal and electrical conductivities prepared by engineered graphene with flat morphology [J]. ACS Nano, 2020, 14(9): 11733−11742. DOI: 10.1021/acsnano.0c04456.

[10] ZHUANG Ya-fang, ZHENG Kun, CAO Xin-yu, et al. Graphene/naphthalene sulfonate composite films with high electrical and thermal conductivities for energy storage and thermal management in nanoscale electronic devices [J]. ACS Applied Nano Materials, 2021, 4(12): 13123 − 13131. DOI: 10.1021/acsanm.1c02643.

[11] LI Liang, MA Zhi-guo, XU Peng-hui, et al. Flexible and alternant-layered cellulose nanofiber/graphene film with superior thermal conductivity and efficient electromagnetic interference shielding [J]. Composites Part A: Applied Science and Manufacturing, 2020, 139: 106134. DOI: 10.1016/j.compositesa.2020.106134.

[12] WANG Yu, WANG Hua-tao, LIU Fei, et al. Flexible printed circuit board based on graphene/polyimide composites with excellent thermal conductivity and sandwich structure [J]. Composites Part A: Applied Science and Manufacturing, 2020, 138: 106075. DOI: 10.1016/j.compositesa. 2020.106075.

[13] GAO Jing-yao, YAN Qing-wei, LV Le, et al. Lightweight thermal interface materials based on hierarchically structured graphene paper with superior through-plane thermal conductivity [J]. Chemical Engineering Journal, 2021, 419: 129609. DOI: 10.1016/j.cej.2021.129609.

[14] DAI Wen, LV Le, LU Ji-bao, et al. A paper-like inorganic thermal interface material composed of hierarchically structured graphene/silicon carbide nanorods [J]. ACS Nano, 2019, 13(2): 1547−1554. DOI: 10.1021/acsnano.8b07337.

[15] MENG Xin, PAN Hui, ZHU Cheng-ling, et al. Coupled chiral structure in graphene-based film for ultrahigh thermal conductivity in both in-plane and through-plane directions [J]. ACS Applied Materials & Interfaces, 2018, 10(26): 22611−22622. DOI: 10.1021/acsami.8b05514.

[16] LV Feng, QIN Meng-meng, ZHANG Fei, et al. High cross-plane thermally conductive hierarchical composite using graphene-coated vertically aligned carbon nanotubes/graphite [J]. Carbon, 2019, 149: 281 − 289. DOI: 10.1016/j.carbon. 2019.04.043.

[17] PENG Li, XU Zhen, LIU Zheng, et al. Ultrahigh thermal conductive yet superflexible graphene films [J]. Advanced Materials, 2017, 29(27): 1700589. DOI: 10.1002/adma. 2017 00589.

[18] AKBARI A, CUNNING B V, JOSHI S R, et al. Highly ordered and dense thermally conductive graphitic films from a graphene oxide/reduced graphene oxide mixture [J]. Matter, 2020, 2(5): 1198 − 1206. DOI: 10.1016/j.matt.2020. 02.014.

[19] WANG Sha-sha, SUN Xian-xian, XU Fan, et al. Strong yet tough graphene/graphene oxide hybrid films [J]. Carbon, 2021, 179: 469−476. DOI: 10.1016/j.carbon.2021.04.052.

[20] YUAN Hong, YE Jiang-lin, YE Chuan-ren, et al. Highly efficient preparation of graphite oxide without water enhanced oxidation [J]. Chemistry of Materials, 2021, 33(5): 1731−1739. DOI: 10.1021/acs.chemmater.0c04505.

[21] LIU Peng-fei, LI Xiao-feng, MIN Peng, et al. 3D lamellar-structured graphene aerogels for thermal interface composites with high through-plane thermal conductivity and fracture toughness [J]. Nano-Micro Letters, 2020, 13(1): 22. DOI: 10.1007/s40820-020-00548-5.

[22] WANG Zi-ming, CAO Yi-yang, PAN De-cai, et al. Vertically aligned and interconnected graphite and graphene oxide networks leading to enhanced thermal conductivity of polymer composites [J]. Polymers, 2020, 12(5): 1121. DOI: 10.3390/polym12051121.

[23] ZHANG Ya-fei, REN Yan-juan, BAI Shu-lin. Vertically aligned graphene film/epoxy composites as heat dissipating materials [J]. International Journal of Heat and Mass Transfer, 2018, 118: 510−517. DOI: 10.1016/j. ijheatmasstransfer.2017.11.014.

[24] LI Hao-liang, DAI Si-chang, MIAO Jie, et al. Enhanced thermal conductivity of graphene/polyimide hybrid film via a novel “molecular welding” strategy [J]. Carbon, 2018, 126: 319−327. DOI: 10.1016/j.carbon.2017.10.044.

[25] MA Lian-ru, WANG Yan-xiang, WANG Yao-yao, et al. Graphene induced carbonization of polyimide films to prepared flexible carbon films with improving-thermal conductivity [J]. Ceramics International, 2020, 46(3): 3332 − 3338. DOI: 10.1016/j.ceramint.2019.10.042.

[26] ZHANG Xin-ru, XIE Xiao-yu, CAI Xin-zhi, et al. Graphene-perfluoroalkoxy nanocomposite with high through-plane thermal conductivity fabricated by hot-pressing [J]. Nanomaterials (Basel, Switzerland), 2019, 9(9): 1320. DOI: 10.3390/nano9091320.

[27] WU Xian, LI Hao-liang, CHENG Kui, et al. Modified graphene/polyimide composite films with strongly enhanced thermal conductivity [J]. Nanoscale, 2019, 11(17): 8219 − 8225. DOI: 10.1039/c9nr02117e.

[28] YUAN Guang-jie, XIE Jie-fei, LI Hao-hao, et al. Thermally reduced graphene oxide/carbon nanotube composite films for thermal packaging applications [J]. Materials (Basel, Switzerland), 2020, 13(2): 317. DOI: 10.3390/ma13020317.

[29] REN Yan-juan, REN Liu-cheng, LI Jia-xiong, et al. Enhanced thermal conductivity in polyamide 6 composites based on the compatibilization effect of polyether-grafted graphene [J]. Composites Science and Technology, 2020, 199: 108340. DOI: 10.1016/j.compscitech.2020.108340.

[30] WANG Ke, LI Meng-xiong, ZHANG Jia-jia, et al. Polyacrylonitrile coupled graphite oxide film with improved heat dissipation ability [J]. Carbon, 2019, 144: 249 − 258. DOI: 10.1016/j.carbon.2018.12.027.

[31] ZOU Rui, LIU Feng, HU Ning, et al. Graphene/graphitized polydopamine/carbon nanotube all-carbon ternary composite films with improved mechanical properties and through-plane thermal conductivity [J]. ACS Applied Materials & Interfaces, 2020, 12(51): 57391−57400. DOI: 10.1021/ acsami.0c18373.

[32] XIA Peng-hui, LI Hao, WANG Yun-jing, et al. Processing aramid nanofiber/modified graphene oxide hydrogel into ultrastrong nanocomposite film [J]. Applied Surface Science, 2021, 545: 149004. DOI: 10.1016/j.apsusc.2021.149004.

[33] WEI Kun-xia, JIA Fei-long, WEI Wei, et al. Flexible nanotwinned graphene/copper composites as thermal management materials [J]. ACS Applied Nano Materials, 2020, 3(5): 4810−4817. DOI: 10.1021/acsanm.0c00844.

[34] VU M C, MANI D, JEONG T H, et al. Nacre-inspired nanocomposite papers of graphene fluoride integrated 3D aramid nanofibers towards heat-dissipating applications [J]. Chemical Engineering Journal, 2022, 429: 132182. DOI: 10.1016/j.cej.2021.132182.

[35] ZHAO Xiao-meng, LI Wei, WANG Yun-jing, et al. Bioinspired modified graphite film with superb mechanical and thermoconductive properties [J]. Carbon, 2021, 181: 40−47. DOI: 10.1016/j.carbon.2021.05.019.

[36] LIU Zheng, WANG Qin-sheng, HOU Lin-lin, et al. Ultralight, ultraflexible, anisotropic, highly thermally conductive graphene aerogel films [J]. Molecules, 2021, 26(22): 6867. DOI: 10.3390/molecules26226867.

[37] ZHANG Fei, FENG Yi-yu, QIN Meng-meng, et al. Stress controllability in thermal and electrical conductivity of 3D elastic graphene-crosslinked carbon nanotube sponge/polyimide nanocomposite [J]. Advanced Functional Materials, 2019, 29(25): 1901383. DOI: 10.1002/adfm.201901383.

[38] KONG Qing-qiang, LIU Zhuo, GAO Jian-guo, et al. Hierarchical graphene-carbon fiber composite paper as a flexible lateral heat spreader [J]. Advanced Functional Materials, 2014, 24(27): 4222 − 4228. DOI: 10.1002/adfm.201304144.

[39] FENG Wei, LI Jian-peng, FENG Yi-yu, et al. Enhanced cross-plane thermal conductivity and high resilience of three-dimensional hierarchical carbon nanocoil-graphite nanocomposites [J]. RSC Advances, 2014, 4(20): 10090 − 10096. DOI: 10.1039/C3RA45647A.

[40] INAGAKI M, OHTA N, HISHIYAMA Y. Aromatic polyimides as carbon precursors [J]. Carbon, 2013, 61: 1−21. DOI: 10.1016/j.carbon.2013.05.035.

[41] HUANG Cong, HU Ai-ping, LI Yan-hua, et al. Room temperature ultrafast synthesis of N- and O-rich graphene films with an expanded interlayer distance for high volumetric capacitance supercapacitors [J]. Nanoscale, 2019, 11(35): 16515−16522. DOI: 10.1039/c9nr06001d.

[42] HUANG Cong, TANG Qun-li, FENG Qiu-shui, et al. Achieving ultrahigh volumetric performance of graphene composite films by an outer−inner dual space utilizing strategy [J]. Journal of Materials Chemistry A, 2020, 8(19): 9661−9669. DOI: 10.1039/c9ta13585e.

[43] ZHAO Xin, HUANG Cong, TANG Qun-li, et al. A simple approach towards highly dense graphene films for high volumetric performance supercapacitors [J]. Chem Electro Chem, 2022, 9(1): e202101451. DOI: 10.1002/celc.202101451.

[44] LI Yan-hua, ZHU Yan-fei, JIANG Gao-peng, et al. Boosting the heat dissipation performance of graphene/polyimide flexible carbon film via enhanced through-plane conductivity of 3D hybridized structure [J]. Small, 2020, 16(8): 1903315. DOI: 10.1002/smll.201903315.

[45] LEE H, RHO J, MESSERSMITH P B. Facile conjugation of biomolecules onto surfaces via mussel adhesive protein inspired coatings [J]. Advanced Materials, 2009, 21(4): 431−434. DOI: 10.1002/adma.200801222.

[46] CAO Ying-ze, ZHANG Xiao-yong, TAO Lei, et al. Mussel-inspired chemistry and Michael addition reaction for efficient oil/water separation [J]. ACS Applied Materials & Interfaces, 2013, 5(10): 4438−4442. DOI: 10.1021/am4008598.

[47] ZOU Rui, LIU Feng, HU Ning, et al. 1-Pyrenemethanol derived nanocrystal reinforced graphene films with high thermal conductivity and flexibility [J]. Nanotechnology, 2020, 31(6): 065602. DOI: 10.1088/1361-6528/ab51c5.

[48] MIAO Jie, LI Hao-liang, QIU Han-xun, et al. Graphene/PANI hybrid film with enhanced thermal conductivity by in situ polymerization [J]. Journal of Materials Science, 2018, 53(12): 8855−8865. DOI: 10.1007/s10853-018-2112-z.

[49] ZOU Rui, LIU Feng, HU Ning, et al. Carbonized polydopamine nanoparticle reinforced graphene films with superior thermal conductivity [J]. Carbon, 2019, 149: 173−180. DOI: 10.1016/j.carbon.2019.04.038.

[50] YUAN H C, LEE C Y, TAI N H. Extremely high thermal conductivity of nanodiamond-polydopamine/thin-layer graphene composite films [J]. Composites Science and Technology, 2018, 167: 313−322. DOI: 10.1016/j.compscitech.2018.08.010.

[51] HECKMANN A, FROMM O, RODEHORST U, et al. New insights into electrochemical anion intercalation into carbonaceous materials for dual-ion batteries: Impact of the graphitization degree [J]. Carbon, 2018, 131: 201−212. DOI: 10.1016/j.carbon.2018.01.099.

[52] NIU Yong-an, FANG Qing-hong, ZHANG Xin, et al. Structural evolution, induced effects and graphitization mechanism of reduced graphene oxide sheets/polyimide composites [J]. Composites Part B: Engineering, 2018, 134: 127−132. DOI: 10.1016/j.compositesb.2017.09.047.

[53] WANG Chong, XIAO Bo, DING Yi-hong. Theoretical investigation on the healing mechanism of divacancy defect in graphene growth by reaction with ethylene and acetylene [J]. New Journal of Chemistry, 2013, 37(3): 640−645. DOI: 10.1039/c2nj40915a.

[54] BOTARI T, PAUPITZ R, ALVES DA SILVA AUTRETO P, et al. Graphene healing mechanisms: A theoretical investigation [J]. Carbon, 2016, 99: 302−309. DOI: 10.1016/j.carbon.2015.11.070.

[55] WANG Nan, SAMANI M K, LI Hu, et al. Tailoring the thermal and mechanical properties of graphene film by structural engineering [J]. Small, 2018, 14(29): 1801346. DOI: 10.1002/smll.201801346.

[56] HUANG Hao-guang, MING Xin, WANG Ya-zhe, et al. Polyacrylonitrile-derived thermally conductive graphite film via graphene template effect [J]. Carbon, 2021, 180: 197−203. DOI: 10.1016/j.carbon.2021.04.090.

(Edited by ZHENG Yu-tong)

中文导读

具有改进的导热性能和力学性能的3D石墨烯/聚酰亚胺纤维框架

摘要：电子元器件的集成化和柔性器件的普及，对热管理材料的散热能力和综合力学性能提出了更高要求。本文通过预氧化和氨基化对聚酰亚胺(PI)纤维进行改性，获得表面活性较强的PDA@OPI纤维，将其与氧化石墨烯(GO)充分混合，形成GO-PDA@OPI混合浆料。随后采用蒸发、碳化、石墨化和机械压实等工艺，制备得到具有3D长程互连结构的G-gPDA@OPI复合薄膜。PDA@OPI纤维通过构成稳定的共价键将相邻的GO片“焊接”在一起，有利于石墨化样品中负载的传递和应力的耗散。同时，这种增强的界面相互作用还显著促进了GO和PI纤维在石墨化过程中的协同效应，以此提高石墨产品的结晶度。另外，PDA@OPI纤维还为热处理进程中因含氧基团分解而产生的气体提供逸出通道，从而使GO片的膨胀效应得到抑制。结果显示，当PDA@OPI纤维的添加量为30%时，G-gPDA@OPI复合薄膜的拉伸强度、极限应变率以及热导率分别达到78.5 MPa，19.4%，1028 W/(m·K)，表现出优异的柔韧性和高回弹率。

关键词：石墨烯薄膜；改性聚酰亚胺纤维；聚多巴胺；热导率；力学性能